AD A 130462

(2)

NRL Memorandum Report 5119

# Small Scale Structure in the Earth's Ionosphere: Theory and Numerical Simulation


S. T. ZALESAK

*Geophysical and Plasma Dynamics Branch*
*Plasma Physics Division*


July 15, 1983

Combined texts of two invited lectures presented at the Theory Institute in Solar-Terrestrial Physics, Boston College, Chestnut Hill, Massachusetts, August 1982.


This research was sponsored by the Defense Nuclear Agency under Subtask S99QMXBC, work unit 00067, work unit title "Plasma Structure Evolution," and by the Office of Naval Research.




NAVAL RESEARCH LABORATORY
Washington, D.C.

| REPORT DOCUMENTATION PAGE | | READ INSTRUCTIONS BEFORE COMPLETING FORM |
|---|---|---|
| 1. REPORT NUMBER<br>NRL Memorandum Report 5119 | 2. GOVT ACCESSION NO. | 3. RECIPIENT'S CATALOG NUMBER |
| 4. TITLE (and Subtitle)<br>SMALL SCALE STRUCTURE IN THE EARTH'S IONOSPHERE: THEORY AND NUMERICAL SIMULATION | | 5. TYPE OF REPORT & PERIOD COVERED<br>Interim report on a continuing NRL problem.<br>6. PERFORMING ORG. REPORT NUMBER |
| 7. AUTHOR(s)<br>S. T. Zalesak | | 8. CONTRACT OR GRANT NUMBER(s) |
| 9. PERFORMING ORGANIZATION NAME AND ADDRESS<br>Naval Research Laboratory<br>Washington, DC 20375 | | 10. PROGRAM ELEMENT, PROJECT, TASK AREA & WORK UNIT NUMBERS<br>62715H; 61153N; RR033-02-44; 47-0889-0-3; 47-0883-0-3 |
| 11. CONTROLLING OFFICE NAME AND ADDRESS<br>Defense Nuclear Agency, Washington, DC 20305<br>Office of Naval Research, Arlington, VA 22217 | | 12. REPORT DATE<br>July 15, 1983<br>13. NUMBER OF PAGES<br>46 |
| 14. MONITORING AGENCY NAME & ADDRESS (if different from Controlling Office) | | 15. SECURITY CLASS. (of this report)<br>UNCLASSIFIED<br>15a. DECLASSIFICATION/DOWNGRADING SCHEDULE |

16. DISTRIBUTION STATEMENT (of this Report)

Approved for public release; distribution unlimited.

17. DISTRIBUTION STATEMENT (of the abstract entered in Block 20, if different from Report)

18. SUPPLEMENTARY NOTES

This research was sponsored by the Defense Nuclear Agency under Subtask S99QMXBC, work unit 00067, work unit title "Plasma Structure Evolution," and by the Office of Naval Research.

Combined texts of two invited lectures presented at the Theory Institute in Solar-Terrestrial Physics, Boston College, Chestnut Hill, Massachusetts, August 1982.

19. KEY WORDS (Continue on reverse side if necessary and identify by block number)

Collisional Rayleigh-Taylor instabilities
Ionospheric barium clouds
Equatorial spread F bubbles
Nonlinear differential equations

20. ABSTRACT (Continue on reverse side if necessary and identify by block number)

We describe in qualitative terms the cause and nonlinear evolution of the gradient drift and collisional Rayleigh-Taylor instabilities in the earth's ionosphere, by using the examples of ionospheric barium clouds and equatorial spread F "bubbles" respectively. We then derive the nonlinear differential equations governing these instabilities. Finally, we discuss the numerical solution of these differential equations.

DD FORM 1473, 1 JAN 73 — EDITION OF 1 NOV 65 IS OBSOLETE
S/N 0102-014-6601

## CONTENTS

# SMALL SCALE STRUCTURE IN THE EARTH'S IONOSPHERE: THEORY AND NUMERICAL SIMULATION

## 1. Introduction

It is generally believed that the existence of ionospheric structures with scale sizes of tens of kilometers or smaller can be attributed primarily to the onset and evolution of instabilities of one sort or another. These instabilities can be thought of as being superimposed on, and indeed evolving from, the larger scale ionospheric configuration. Among the numerous such structures it is usually only those that are of reasonably large amplitude or those which cause problems (e.g. communications interference) that attract interest and study. Still, this number is greater than we can reasonably treat here. We shall therefore limit our discussion to two such structures whose physics and evolution we believe we understand reasonably well: 1) the steepening and subsequent recursive splitting of barium clouds released in the ionosphere, driven by the gradient drift instability; and 2) the formation and buoyant rise of low density "bubbles" of plasma in the nighttime equatorial ionosphere, known as equatorial spread F (ESF), driven by the collisional Rayleigh-Taylor instability. Each of these instabilities derive from the same set of plasma fluid equations and the same set of physical approximations, differing only in geometry and in the identity of the driving terms; hence we shall attempt here to unify their description as much as possible. We shall find that one of the characteristics of structures resulting from these instabilities is their tendency to be "field aligned", that is, for the plasma gradients and velocities parallel to the magnetic field to be much smaller than those perpendicular to the magnetic field. Our discussion will therefore focus on plasma motion perpendicular to the ambient magnetic field.

In Figure 1 we show a photograph of the Spruce event, a barium cloud released at 188 km altitude in February of 1971, 24 minutes after release. The cloud was originally released as a gaussian distribution of neutral barium which was subsequently photoionized by sunlight. In the very center of the photograph, our line of sight is parallel to the magnetic field lines at the cloud altitude, revealing the fine scale structure (termed "striations") that has evolved from this originally

Manuscript approved April 27, 1983.

nearly gaussian distribution of plasma. In Figure 2 we show a sketch of what we believe to be the typical evolution of a barium cloud like Spruce, dervived from experimental observations and numerical simulations. The inital steepening of the top of the two-dimensinal cloud is caused by the buildup of polarization charge on its sides, causing the high density center of the cloud to $\underset{\sim}{E} \times \underset{\sim}{B}$ drift in the direction of the neutral wind to a greater extent than the low density edges. As the plasma gradient on the top of the cloud becomes steeper, the growth rate of the gradient drift instability (to be described later) active there becomes larger and eventually small perturbations on this gradient are amplified into visible ripples, which in turn evolve into finger-like structures. Each of the strucutes emerging from the steepened edge of the cloud then evolve into smaller clouds, and the process begins again, resulting in a cascade of recursively decreasing scale sizes until the instability is stopped by dissipation or other mechanisms which act more effectively on the smaller space scales.

In Figure 3 we show maps of 1-m irregularities taken from Tsunoda (1981) at the earth's magnetic equator during equatorial spread F (ESF). These irregularities have been shown to be closely associated with "bubbles" or regions of large electron density depletion in the equatorial ionosphere, and can be thought of as at least a partial map of the locations of severe electron density depletion. In Figure 4 we show the results of a numerical simulation from Zalesak, et al. (1982), showing the time evolution of electron density contours at the earth's equator. The equatorial ionosophere was originally laminar with a maximum in electron density at 430 km altitude. A sinusoidal perturbation was applied in the east-west direction. The results show that the observed "bubbles" consist of low density plasma which has been transported from very low altitudes up through the F2 peak and beyond by the nonlinear evolution of the collisional Rayleigh-Taylor instability. The westward and eastward tilts of the bubble are due to an eastward neutral wind blowing at the equator coupled along magnetic field lines to background ionization (e.g., E regions) at higher and lower latitudes. Note that the various tilts of the bubbles in Figures 3 and 4 are consistent when allowance is made for the reversed abscissae in the two plots.

In Section 2 we shall present a qualitive, physical description of the instabilities active in ionospheric barium cloud and equatorial spread F (ESF) cases. In Section 3 we derive the set of equations describing the motion of ionospheric plasma in general, and the evolution of barium clouds and ESF bubbles in particular. In Section 4 we discuss the simplifications made in constructing a mathematical representation of the physical system. In Section 5 we derive and summarize the equations describing the "simplest case" geometries and assumptions for each of the instabilities. Finally, in Sections 6 through 8, we treat the numerical integration of these differential equations.

## 2. The Gradient Drift/Collisional Rayleigh-Taylor Instability

In this section we shall attempt to give a qualitative physical picture of the gradient drift and collional Rayleigh-Taylor instabilities, both of which are caused by the differential motion of ions and electrons perpendicular to the magnetic field. We consider a two-dimensional x-y plane perpendicular to the ambient magnetic field $\underset{\sim}{B}$. A plasma species $\alpha$ in this plane embedded in a neutral gas will respond to an external force perpendicular to $\underset{\sim}{B}$, $\underset{\sim}{F}_{\alpha\perp}$, in two ways: 1) by drifting in a direction perpendicular to both $\underset{\sim}{B}$ and $\underset{\sim}{F}_{\alpha\perp}$ (Hall mobility) and 2) usually to a lesser extent, by drifting in a direction parallel to $\underset{\sim}{F}_{\alpha\perp}$ (Pedersen mobility). We shall explicity derive these drifts in Section 3. We shall take our plasma to consist of a single ion species, denoted by subscript i, and of electrons, denoted by subscript e. The instabilities under discussion result from the fact that the ions and electrons drift with different velocities and directions in response to the same external force. In regions where plasma density gradients exist, this difference in velocities causes polarization charge to be created in our originally neutral plasma, which in turn produces a polarization electric field. The plasma drift associated with the electric field will cause growth of a perturbation when the plasma gradient is properly aligned.

In Figure 5 we show contours of contant plasma density n in the two-dimensional x-y plane, where we assume the magnetic field $\underset{\sim}{B}$ to be aligned along the positive z axis. Depicted is a one-dimensional "slab" of plasma n(y) such that n maximizes at $y = y_o$, superimposed on which is a sinusoidal perturbation proportional to sin kx, where k is a wavenumber. Either a downward-directed gravational acceleration (in the collisional Rayleigh-Taylor instability) or a downward-directed neutral wind (in the gradient drift instability) will cause the ions to drift leftward relative to the electrons, leaving polarization charge where the relative drift has components parallel to the density gradient, as indicated in Figure 5. This polarization charge induces a polarization electric field $\underset{\sim}{E}_p$, which in turn induces an additional plasma drift in the $\underset{\sim}{E}_p \times \underset{\sim}{B}$ direction. This drift is such as to enhance the perturbation for $y < y_o$ (instability), as seen in Figure 5. In their most simplified geometries the linear growth rates $\gamma$ for the gradient drift and collisional Rayleigh-Taylor *instabilities are*

$$\gamma = - \underset{\sim}{U}_n \cdot \frac{\nabla n}{n} \qquad \text{(gradient drift)} \qquad (1)$$

$$\gamma = - \underset{\sim}{g} \cdot \frac{\nabla n}{n} \nu_{in}^{-1} \qquad \text{(Rayleigh-Taylor)} \qquad (2)$$

where $\nu_{in}$ is the ion-neutral collision frequency. We note here that the gradient drift instability may be thought of as being driven by an ambient electric field simply by performing a Lorentz transformation into the rest frame of the neutral gas.

The above picture of the early (linear) stage of the instability evolution is quite informative, but unfortunately falls short of illuminating the complex nonlinear evolution of barium clouds and equatorial spread F "bubbles". In the next section we derive the equations necessary for a complete nonlinear description of these phenomena, which in general require numerical techniques for their solution.

## 3. The Motion of Ionospheric Plasma

We shall be concerned here with the motion of plasma consisting of ions and electrons in the presence of a neutral gas and magnetic field $\underset{\sim}{B}$, subject to an external force. We shall also be interested in the electric current $\underset{\sim}{J}$ arising from the differential motion of thevarious species comprising the plasma. In the course of deriving the equations we shall make some assumptions which are crucial to the model:

1) We shall assume the plasma can be adequately described by the fluid approximation. This assumes that the effective collision rate of each plasma species with itself is sufficiently high to maintain near Maxwellian distribution functions on time scales short compared to the times of interest, and is well satisfied for the plasmas we treat here.

2) We shall assume that the electric fields $\underset{\sim}{E}$ are electrostatic (i.e., $\nabla \times \underset{\sim}{E} = 0$) and hence can be described using a scalar potential $\phi$ such that $\underset{\sim}{E} = - \nabla \phi$. Note that this implies $\partial \underset{\sim}{B}/\partial t = 0$. The validity of this assumption can be related to the fact that the Alfven velocity is much larger than any other propagation speeds of interest for the plasmas we treat here. The assumption is also checked a posteriori by verifying that the calculated currents and displacement currents produce negligible time variations in $\underset{\sim}{B}$ which in turn produce negligible $\nabla \times \underset{\sim}{E}$.

3) We assume plasma quasi-neutrality; that is,

$$\sum n_i q_i = n_e e \tag{3}$$

where n is number density, q is ion species charge, e is the electron charge, the subscripts i and e refer to ions and electrons respectively, and the sum is taken over all ion species. This assumption is a statement that the Debye length is small compared to all length scales of interest, and again can be verified a posteriori by evaluating $\nabla \cdot \underset{\sim}{E}$. Note that this assumption implies that $\nabla \cdot \underset{\sim}{J} = 0$, where $\underset{\sim}{J}$ is the electric current. In addition to the above there are some other assumptions which, while they are not essential to the basic model, are nonetheless valid for many of the physical situations which we shall treat and impart a simplicity which we shall find convenient here:

4) We shall assume the electrostatic potential $\phi$ to be constant along magnetic field lines. As we shall see later, the electrical conductivity along magnetic field lines is much greater that that perpendicular to magnetic field lines, meaning that appreciable differences in potential along a field line will quickly be reduced by the resultant current. This assumption will break down for sufficiently small scale lengths perpendicular to the magnetic field, and for sufficiently large distances along the magnetic field.

5) We shall assume that the inertial terms in the plasma species momentum equations, i.e., the left hand side of Equation (5), are negligible with respect to the other terms in the equation. This assumption is justified whenever the time scales of interest are longer than the mean time between collisions for ions.

6) We shall neglect all collisions between species except those between ions and the neutral gas. This is justified simply by an evaluation of the magnitudes of the terms involved.

7) We shall ignore production and loss terms which may appear as sources and sinks in the plasma continuity equations as a result of chemistry, photoionization, etc.

Assumptions (4) through (7) above, although made in this paper, are not necessary within the theoretical and computational framework we have developed, and adequate means exist to delete them, if necessary.

The continuity and momentum equations describing plasma species $\alpha$ are:

$$\frac{\partial n_\alpha}{\partial t} + \nabla \cdot (n \underset{\sim}{v}_\alpha) = 0 \qquad (4)$$

$$(\frac{\partial}{\partial t} + \underset{\sim}{v}_\alpha \cdot \nabla)\, \underset{\sim}{v}_\alpha = \frac{q_\alpha}{m_\alpha}(\underset{\sim}{E} + \frac{\underset{\sim}{v}_\alpha \times \underset{\sim}{B}}{c}) - \nu_{in}(\underset{\sim}{v}_\alpha - \underset{\sim}{U}_n) -$$

$$- \frac{\nabla P_\alpha}{n_\alpha m_\alpha} + \underset{\sim}{g} \tag{5}$$

where the subscript $\alpha$ denotes the plasma species (i for ions, e for electrons, for example), n is the species number density, $\underset{\sim}{v}$ is the species fluid velocity, P is pressure, $\underset{\sim}{E}$ is the electric field, $\underset{\sim}{g}$ is the gravitational acceleration, q is the species charge, $\nu_{\alpha n}$ is the species collision frequency with the neutral gas, $\underset{\sim}{U}_n$ is the neutral wind velocity, c is the speed of light, and m is the species particle mass. We can rewrite this equation as

$$\underset{\sim}{F}_\alpha / m_\alpha + \frac{q_\alpha}{m_\alpha c}(\underset{\sim}{v}_\alpha \times \underset{\sim}{B}) - \nu_{\alpha n}\, \underset{\sim}{v}_\alpha = 0 \tag{6}$$

where

$$\underset{\sim}{F}_\alpha \equiv q_\alpha \underset{\sim}{E} + m_\alpha g + \nu_{\alpha n}\, m_\alpha \underset{\sim}{U}_n - \nabla P_n / n_\alpha$$

$$- (\frac{\partial}{\partial t} + \underset{\sim}{v}_\alpha \cdot \nabla)\, \underset{\sim}{v}_\alpha\, m_\alpha \tag{7}$$

If we place ourselves in a Cartesian coordinate system in which $\underset{\sim}{B}$ is aligned along the z axis, and if we treat $\underset{\sim}{F}_\alpha$ as a given quantity then a componentwise evaluation of Equation (6) yields a set of three equations in three unknowns, the three components of $\underset{\sim}{v}_\alpha$. The formal solution is

$$\underset{\sim}{v}_{\alpha\perp} = k_{1\alpha}\, \underset{\sim}{F}_{\alpha\perp} + k_{2\alpha}\, \underset{\sim}{F}_{\alpha\perp} \times \hat{z} \tag{8}$$

$$\underset{\sim}{v}_{\alpha\parallel} = k_{o\alpha}\, \underset{\sim}{F}_{\parallel} \tag{9}$$

where

$$k_{1\alpha} = \frac{\nu_{\alpha n}}{\Omega_\alpha} \frac{c}{|q_\alpha B|} \left[1 - \frac{(\nu_{\alpha n}/\Omega_\alpha)^2}{1 + (\nu_{\alpha n}/\Omega_\alpha)^2}\right] \tag{10}$$

$$k_{2\alpha} = \frac{c}{q_\alpha B} \left[1 - \frac{(\nu_{\alpha n}/\Omega_\alpha)^2}{1 + (\nu_{\alpha n}/\Omega_\alpha)^2}\right] \tag{11}$$

$$k_{o\alpha} = (m_\alpha \nu_{\alpha n})^{-1} \tag{12}$$

$$\hat{z} \equiv \underset{\sim}{B}/|B| \tag{13}$$

$$\Omega_\alpha \equiv \left|\frac{q_\alpha B}{m_\alpha c}\right| \tag{14}$$

The vector subscripts $\perp$ and $\parallel$ refer to the components of the vector which are perpendicular and parallel respectively to $\hat{z}$. The quantities $k_1$, $k_2$, and $k_o$ above are referred to as the Pedersen, Hall, and direct mobilities respectively. It should be pointed out that Equations (8) and (9) are only truly closed form expressions when the inertial terms (the last term on the right hand side of Equation (7)) are neglected, an assumption we have made previously. Typical ranges for collision frequencies are: $\nu_{in} \sim 30\ \text{sec}^{-1}$, $\nu_{en} \sim 800\ \text{sec}^{-1}$ at 150 km altitude; and $\nu_{in} \sim 10^{-1}\text{sec}^{-1}$, $\nu_{en} \sim 1\ \text{sec}^{-1}$ at 500 km altitude.

As we will see later, we will use the concept of "layers" to distinguish the various ion species, so for the moment we can consider only a single ion species, denoted by subscript i, and the associated electrons, denoted by subscript e. We will also consider only singly charged ions so that $q_i = e$ and $q_e = -e$. Noting that $\nu_{en}/\Omega_e \approx 0$ we obtain

$$k_{1i} = \frac{\nu_{in}}{\Omega_i} R_i \frac{c}{e|B|} \tag{15}$$

$$k_{1e} = 0 \tag{16}$$

$$k_{2i} = R_i \frac{c}{eB} \tag{17}$$

$$k_{2e} = -\frac{c}{eB} \tag{18}$$

where

$$R_i \equiv (1 + \nu_{in}^2/\Omega_i^2)^{-1} \tag{19}$$

We now define the perpendicular current

$$\underset{\sim}{J}_\perp \equiv \sum_\alpha n_\alpha q_\alpha v_{\alpha\perp} \tag{20}$$

Substituting Equations (15) through (18) and (8) into Equation (20), and using the quasi-neutrality approximation

$$n_i \approx n_e \equiv n \tag{21}$$

we obtain

$$\begin{aligned} \underset{\sim}{J}_\perp = {} & \frac{\nu_{in}}{\Omega_i} R_i \frac{nc}{|B|} \underset{\sim}{F}_{i\perp} \\ & + \frac{nc}{B} (R_i \underset{\sim}{F}_{i\perp} + \underset{\sim}{F}_{e\perp}) \times \hat{z} \end{aligned} \tag{22}$$

For the barium cloud and equatorial spread F (ESF) problems we shall treat here, we shall only consider neutral winds, electric fields, and gravity as external forces. Hence

$$\underset{\sim}{F}_{i\perp} = e \underset{\sim}{E}_\perp + m_i \underset{\sim}{g}_\perp + \nu_{in} m_i \underset{\sim}{U}_{n\perp} \tag{23}$$

$$\underset{\sim}{F}_{e\perp} = - e \underset{\sim}{E}_\perp + m_e \underset{\sim}{g}_\perp \tag{24}$$

Note that we have neglected the small term $\nu_{en} m_e$ in Equation (24).
We obtain

$$\underset{\sim}{J}_{\perp} = \frac{\nu_{in}}{\Omega_i} R_i \frac{nc}{|B|} (e \underset{\sim}{E}_{\perp} + m_i \underset{\sim}{g}_{\perp} + \nu_{in} m_i \underset{\sim}{U}_{n\perp})$$

$$+ R_i \frac{nc}{B} \left[e \underset{\sim}{E}_{\perp} (1 - R_i^{-1}) + m_i + \frac{m_e}{R_i}) \underset{\sim}{g}_{\perp} + \nu_{in} m_i \underset{\sim}{U}_{n\perp}\right] \times \hat{z} \tag{25}$$

Since $0.01 < R_i < 1.0$ we may neglect $m_e/R_i$ with respect to $m_i$. Defining the Pedersen conductivity

$$\sigma_p \equiv R_i \frac{\nu_{in}}{\Omega_i} \frac{nce}{|B|} \tag{26}$$

and noting that $1 - R_i^{-1} = - \nu_{in}{}^2/\Omega_i{}^2$ we obtain

$$\underset{\sim}{J}_{\perp} = \sigma_p \left[\underset{\sim}{E}_{\perp} + \frac{m_i}{e} \underset{\sim}{g}_{\perp} + \nu_{in} \frac{m_i}{e} \underset{\sim}{U}_{n\perp}\right.$$

$$\left. + \left( - \frac{\nu_{in}}{\Omega_i} \underset{\sim}{E}_{\perp} + \frac{\Omega_i m_i}{\nu_{in} e} \underset{\sim}{g}_{\perp} + \Omega_i \frac{m_i}{e} \underset{\sim}{U}_{n\perp}\right) \times \hat{z}\right] \tag{27}$$

Our need for an expression for $\underset{\sim}{J}_{\perp}$ stems from our need for its divergence to evaluate $\nabla \cdot \underset{\sim}{J}$ ( = 0 by quasi-neutrality), as we shall see in the next section.

## 4. Model Simplification and Mathematical Representation

We shall model our physical system using a simplified model as depicted in Figure 6. The magnetic field lines are assumed to be straight, to be aligned along the z axis of our cartesian coordinate system, and to terminate in insulators at $z = \pm \infty$. The plasma of interest is threaded by these magnetic field lines, and is divided into thin planes or "layers" of plasma perpendicular to the magnetic field. Since we have neglected collisions between different plasma species, we may use the device of layers to treat multiple ion species at a single point in space simply by allowing multiple layers to occupy the same plane in space, one for each ion species. In this way a "layer" consists only of a single ion species and its associated electrons.

Our quasi-neutrality assumption demands that

$$\nabla \cdot \underset{\sim}{J} = \frac{\partial}{\partial x} J_x + \frac{\partial}{\partial y} J_y + \frac{\partial}{\partial z} J_z = 0 \tag{28}$$

Integrating Equation (28) along z and noting from Figure 6 that $J_z$ vanishes at $z = \pm \infty$ we obtain

$$\int_{-\infty}^{+\infty} \nabla_\perp \cdot J_\perp \, dz = 0 \tag{29}$$

where

$$\nabla_\perp \equiv \hat{x} \frac{\partial}{\partial x} + \hat{y} \frac{\partial}{\partial y} \tag{30}$$

From our model as depicted in Figure 6 we may approximate the integral in Equation (29) by a discrete sum

$$\sum_{k=1}^{N} \nabla_\perp \cdot \underset{\sim}{J}_{\perp k} \, \Delta z_k = 0 \tag{31}$$

where the subscript k refers to the layer number, N is the total number of layers in the system, and $\Delta z_k$ is the thickness of layer k measured along the magnetic field line. By our assumption of equipotential magnetic field lines and electrostatic electric fields

$$\underset{\sim}{E}_{\perp k}(x,y) = - \nabla_\perp \phi(x,y) \text{ for all } k \tag{32}$$

Then Equation (31) becomes

$$\nabla_\perp \cdot \left[\sum_{k=1}^{N} (\Sigma_{pk})\nabla_\perp \phi\right] + \sum_{k=1}^{N} H_k = \sum_{k=1}^{N} \nabla_\perp \cdot \underset{\sim}{J}^{ext}_{\perp k} \tag{33}$$

where

$$\Sigma_{pk} \equiv \sigma_{pk}\, \Delta z_k \tag{34}$$

$$\begin{aligned} H_k &\equiv - \frac{\partial}{\partial x}\left(\frac{\nu_{in}}{\Omega_i} \Sigma_p \frac{\partial \phi}{\partial y}\right)_k + \frac{\partial}{\partial y}\left(\frac{\nu_{in}}{\Omega_i} \Sigma_p \frac{\partial \phi}{\partial x}\right)_k \\ &= - \frac{\partial \phi}{\partial y} \frac{\partial}{\partial x}\left(\frac{\nu_{in}}{\Omega_i} \Sigma_p\right)_k + \frac{\partial \phi}{\partial x} \frac{\partial}{\partial y}\left(\frac{\nu_{in}}{\Omega_i} \Sigma_p\right)_k \end{aligned} \tag{35}$$

$$\begin{aligned} \underset{\sim}{J}^{ext}_{\perp k} \equiv \Sigma_{pk} &\Big[\frac{m_i}{e} \underset{\sim}{g}_\perp + \nu_{in} \frac{m_i}{e} \underset{\sim}{U}_{n\perp} \\ &+ \Big(\frac{\Omega_i m_i}{\nu_{in} e} \underset{\sim}{g}_\perp + \Omega_i \frac{m_i}{e} \underset{\sim}{U}_\perp\Big) \times \hat{z}\Big]_k \end{aligned} \tag{36}$$

and the subscript k denoting layer number on terms within parenthesis operates on all terms within those parentheses. Equation (33) is a second order elliptic partial differential equation for $\phi(x,y)$, subject to boundary conditions on $\phi$. Our reason for writing Equation (33) in the form we did is related to the following picture of the physics. The external forces acting on a plasma, in this case gravity and a neutral wind collision term, will induce a current to flow. In general this current will <u>not</u> satisfy $\nabla \cdot \underset{\sim}{J} = 0$, meaning that in certain regions there will be a build-up of polarization charge, resulting in an electric field which causes secondary currents to flow. Over time scales <u>much</u> shorter than those of interest here, a quasi-steady state is reached such that subsequent plasma motion is well described by $\nabla \cdot \underset{\sim}{J}_\perp = 0$. In this physical picture the electric field represents the <u>response</u> of the plasma to a <u>given</u> externally driven current system. Thus the right hand side of the Equation (33) may be regarded as the "known" divergence of the external current, which we shall denote below by R, and the left hand side regarded as a differential operator L operating on $\phi$:

$$L\phi = R \tag{37}$$

The operator L is a hermitian operator in the limit as the "Hall terms" $H_k$ may be neglected, as is often the case at higher altitudes where $\nu_{in}/\Omega_i$ is small.

## 5. The simplest Case Equations for Barium Clouds and for ESF

The simplest case equations for each of our physical systems are for one level only, i.e., N=1, and for altitudes such that terms of order $(\nu_{in}/\Omega_i)^2$ may be neglected with respect to terms of order $(\nu_{in}/\Omega_i)$. We also treat only one external force for each case, and align that force along one of the coordinate axes. Since we have only one level, we drop the subscript k.

For barium clouds, we assume $\underset{\sim}{B}$ to be aligned along the z axis, that the only external force is a neutral wind $\underset{\sim}{U}_n \equiv U_n \hat{y}$.
Then

$$\underset{\sim}{J}_\perp^{ext} = \Sigma_p \left(\nu_{in} \frac{m_i}{e} U_n \hat{y} + \Omega_i \frac{m_i}{e} U_n \hat{x}\right) \tag{38}$$

Since $\Sigma_p$ is already of order $(\nu_{in}/\Omega_i)$, we may neglect the first term with respect to the second. Then

$$\nabla_\perp \cdot \underset{\sim}{J}_\perp^{ext} = \frac{\partial}{\partial x} \left(\Sigma_p \frac{BU_n}{c}\right) \tag{39}$$

where we have used Equation (14).
Noting that H in Equation (33) is of order $(\nu_{in}/\Omega_i)^2$ we obtain

$$\nabla_\perp \cdot (\Sigma_p \nabla_\perp \phi) = \frac{\partial}{\partial x} \left(\Sigma_p \frac{BU_n}{c}\right) \tag{40}$$

For the equatorial spread F case we assume a single plane of plasma located at the magnetic equator such that $\underset{\sim}{B}$ is along the z axis and $\hat{y}$ is "up". Our only external force is gravity $g_\perp = - g\hat{y}$ ($g = + 980$ cm/sec$^2$). Then

$$\underset{\sim}{J}_\perp^{ext} = \Sigma_p \left[- \frac{m_i}{e} g \hat{y} - \frac{\Omega_i}{\nu_{in}} \frac{m_i}{e} g \hat{x}\right] \tag{41}$$

The first term is of order $\nu_{in}/\Omega_i$ times the second and may therefore be neglected. Then

$$\nabla_\perp \cdot \underset{\sim}{J}_\perp^{ext} = - \frac{\partial}{\partial x} (\Sigma_p \frac{Bg}{c\nu_{in}}) \tag{42}$$

Again neglecting H in Equation (33) we obtain

$$\nabla_\perp \cdot (\Sigma_p \nabla_\perp \phi) = - \frac{\partial}{\partial x} \left(\Sigma_p \frac{Bg}{c\nu_{in}}\right) \tag{43}$$

For both the one-layer barium cloud and ESF cases, one may solve either the electron or the ion continuity equations, since quasi-neutrality makes them equivalent (but not identical). For simplicity we choose the electron equation since we may neglect the Pedersen terms there ($\nu_{en}/\Omega_e = 0$).

Summarizing the equations we must solve for each case we get

$$\frac{\partial n_e}{\partial t} = \nabla_\perp \cdot (n_e \underset{\sim}{v}_{e\perp}) = 0 \tag{44}$$

$$\nabla_\perp \cdot (\Sigma_p \nabla_\perp \phi) = \partial S/\partial x \tag{45}$$

$$\underset{\sim}{v}_{e\perp} = - \frac{c}{eB} \underset{\sim}{F}_{e\perp} \times \hat{z} \tag{46}$$

$$\underset{\sim}{F}_{e\perp} = \begin{cases} e\nabla_\perp \phi & \text{for barium clouds} \\ e \nabla_\perp \phi - m_e g\hat{y} & \text{for ESF} \end{cases} \tag{47}$$

$$S = \begin{cases} \Sigma_p \, U_n/c & \text{for barium clouds} \\ - \Sigma_p \, Bg/(c\nu_{in}) & \text{for ESF} \end{cases} \tag{48}$$

$$\Sigma_p = \Delta z \, (\nu_{in}/\Omega_i) nce/B \tag{49}$$

Solution of these equations requires the use of two-dimensional numerical simulation techniques.

## 6. Numerical Simulation: General

We saw in the previous section that in the simplest case for the barium cloud and equatorial spread F (ESF) problems, we can reduce our system to two partial differential equations posed on a two dimensional plane:

$$\frac{\partial n}{\partial t} + \nabla_\perp \cdot (n \, \underset{\sim}{v}_{e\perp}) = 0 \tag{50}$$

$$\nabla_\perp \cdot (\Sigma_p \, \nabla_\perp \, \phi) = \partial S/\partial x \tag{51}$$

where $\Sigma_p$ and S are explicity given functions of n and $\underset{\sim}{v}_{e\perp}$ is an explicity given function of $\phi$. Equation (50) is hyperbolic while Equation (51) is elliptic. Both require the imposition of physically relevant boundary conditions. Conceptually one solves this coupled system of equations as follows. At any given time t, we assume that we know n(x,y,t) and therefore $\Sigma_p(x,y,t)$ and S(x,y,t). We can then solve Equation (51) for its single scalar unknown $\phi(x,y,t)$, given properly specified boundary conditions on $\phi$ and/or its derivatives. Knowing $\phi$ we can compute $\underset{\sim}{v}_{e\perp}(x,y,t)$ explicity. We can then solve Equation (50) for $n(x,y,t + \Delta t)$ where $\Delta t$ is a small time increment. The process is repeated recursively until the solution is advanced to the desired time.

Within the above context several numerical approaches exist for solving this system of coupled partial differential equations: spectral methods, finite element methods, Galerkin methods, and finite difference methods, among others. We have chosen finite difference methods here for reasons of simplicity, computational efficiency, and most importantly because acceptable techniques for solving Equation (50) in the presence of large gradients in n presently exist only within the finite difference domain. Fundamental to finite difference techniques is their use of a "grid", that is, a discrete set of points in space and time denoted by $(x_i, y_i, t^m)$, $1 \leq i \leq NX$, $1 \leq j \leq NY$, $1 \leq n < \infty$ where i, j, m, NX and NY are integers, on which the solution is computed. For instance, the electrostatic potential $\phi(x,y,t)$ at $x = x_i$, $y = y_j$, and $t = t^m$ would be denoted $\phi^m_{ij}$. In Figure 7, we show an example of a finite difference grid in space, and we also show how the grid would look in the case of multiple layers of plasma, although we shall treat only a single layer here. Note that the four "nearest neighbors" of the grid point $(x_i, y_j)$ are the grid points $(x_{i+1}, y_j)$, $(x_{i-1}, y_j)$, $(x_i, y_{j+1})$, and $(x_i, y_{j-1})$. Many finite difference techniques employ what is known as a staggered grid, meaning that different dependent variables (n and $\phi$ for instance) are evaluated on different grids in space and possibly time. We do not employ staggered grids here; all dependent variables are evaluated on exactly the same grid.

Looking at Equations (50) and (51) we see that there is more to distinguish them than just their hyperbolicity and ellipticity respectively. Both equations require the evaluation of spatial derivatives; but Equation (50) requires in addition the evaluation of temporal derivatives. Precisely because we do not yet know the solution at a time later than it has thus far been computed, the treatment of temporal derivatives is qualitatively different from that of spatial derivatives. More importantly, it has been found empirically that it is the numerical treatment of Equation (50) which will "make or break" the solution to the total system of equations. Specifically, Equation (51), once properly discretized (i.e., once the spatial derivatives are properly represented in finite difference form) simply yields a system of linear equations, albeit a very large system. Our experience has been that a number of algorithms will successfully yield a solution to this linear system, although it may be difficult to find one algorithm that will solve the system for all possible physical parameters. Accordingly we shall discuss the numerical treatment of Equation (51) only briefly here, in the next section, and reserve the bulk of our discussion for Equation (50).

## 7. The Numerical Solution of the Potential Equation

As was mentioned in the previous section, the numerical solution of Equation (51) takes place in two stages: 1) the discretization of the spatial derivatives and boundary conditions in finite difference form, resulting in a large linear system of NX • NY equations for the NX • NY unknowns $\phi_{ij}$; and 2) the solution of this large linear system. Equation (51) is discretized as follows

$$[\partial\,(\Sigma\ \partial\phi/\partial x)/\partial x]_{i,j} = \frac{\Sigma_{i+1/2}\ \phi'_{i+1/2} - \Sigma_{i-1/2}\ \phi'_{i-1/2}}{(1/2)(x_{i+1} - x_{i-1})} \tag{52}$$

$$[\partial\,(\Sigma\ \partial\phi/\partial y)/\partial y]_{i,j} = \frac{\Sigma_{j+1/2}\ \phi'_{j+1/2} - \Sigma_{j-1/2}\ \phi'_{j-1/2}}{(1/2)\ (y_{j+1} - y_{j-1})} \tag{53}$$

$$[\partial S/\partial x]_{i,j} = \frac{S_{i+1,j} - S_{i-1,j}}{x_{i+1} + x_{i-1}} \tag{54}$$

where

$$\Sigma_{i+1/2} \equiv (1/2)\ (\Sigma_{i+1,j} + \Sigma_{i,j}) \tag{55}$$

$$\Sigma_{j+1/2} \equiv (1/2)\ (\Sigma_{i,j+1} + \Sigma_{i,j}) \tag{56}$$

$$\phi'_{i+1/2} \equiv (\phi_{i+1,j} - \phi_{i,j})/(x_{i+1} - x_i) \tag{57}$$

$$\phi'_{j+1/2} \equiv (\phi_{i,j+1} - \phi_{i,j})/(y_{j+1} - y_j) \tag{58}$$

The above expressions can be evaluated only for $2 < i < NX - 1$ and for $2 < j < NY - 1$, leaving $(NX-2) \cdot (NY-2)$ equations in $NX \cdot NY-4$ unknowns (note that the corner points of the grid do not appear in the above equations). The missing $2(NX+NY)-8$ equations are derived from the boundary conditions imposed on $\phi$. For instance, the simplest boundary conditions that could be imposed would be Dirichlet, i.e., specification of known values of $\phi$ for the $2(NX+NY)-8$ grid points comprising the perimeter of our grid. Another possibility would be Neumann boundary conditions, which would specify known values of the normal derivative of $\phi$ at the boundary. For instance, the equation

$$(\phi_{N,j} - \phi_{N-1,j})/(x_N - x_{N-1}) = BX_{N-1/2,j} \tag{59}$$

can be thought of as imposing the condition that the normal derivative at the right boundary point $x = (1/2)\ (x_N + x_{N-1})$, $y = y_j$ be equal to $BX_{N-1/2,j}$, the value of which is presumably given.

The solution to this linear system of equations, while by no means a trivial exercise, can be accomplished by a number of algorithms. We have found one and only one algorithm which will yield a solution in all cases, the Stabilized Error Vector Propagation (SEVP) algorithm of Madala (1978). This is a direct solver and can be expensive on a large grid. Iterative solvers with which we have had success include the Chebyshev semi-iterative method of McDonald (1980), and the vectorized incomplete Cholesky conjugate gradient (ICCG) algorithm of Hain (1980), which is an extension of the work of Kershaw (1978).

## 8. The Numerical Solution of the Continuity Equation

The continuity equation is ubiquitous in all of physics. It is simply a statement of the fact that a conserved quantity (mass for instance) can only appear somewhere in space if it comes from somewhere else. As we have noted previously, Eq. (50) is distinguished by the appearance of both spatial and temporal derivatives. We have also noted previously that we intend to treat these spatial and temporal derivatives in distinctly different ways numerically. The formal distinction of spatial and temporal derivatives takes the form of a general numerical technique which has come to be known as the Method of Lines (MOL). In the Method of Lines one simply treats the entire spatial differential operator as some nonlinear operator H operating on the operand or operands of the temporal derivative operator, this case n:

$$\frac{\partial n}{\partial t} = H(n) \tag{60}$$

where

$$H(n) = \nabla_{\perp} \cdot (n \, \underset{\sim}{v}_{e\perp}) \tag{61}$$

Note that $\underset{\sim}{v}_{e\perp}$ is a function of n by Eq. (51) and the definitions of $\Sigma_p$, S, and $\underset{\sim}{v}_{e\perp}$. H is therefore a very complicated nonlinear operator acting on n which involves all of the spatial discretization and definitions implicit in solving Eq. (51), as well (as we shall see) as the spatial finite difference discretization needed to represent the operator $\nabla_{\perp}$ for Eq. (50). Nonetheless this formalism considerably simplifies our task, for it allows us to cleanly separate out our treatment of the temporal derivatives. We note that now Eq. (60) is simply an ordinary differential equation (ODE) for which a wide variety of numerical integration techniques, known as "ODE solvers", exist. Actually, as we shall see later Eq. (60) and (61) actually represents a system of ODE's, one for each spatial grid point, which are coupled to each other through spatial finite differences and through the solution of the elliptic equation (51). We are fortunate here in that our system of ODE's never becomes stiff (i.e., there are no solutions with time scales much shorter than those of physical interest), and hence we have no need of the more sophisticated numerical techniques available for such situations. The solvers actually in use in the present versions of our simulation codes are as follows:

Leapfrog - Trapezoidal:

$$n' = n(t-\Delta t) + 2H(n(t))\,\Delta t \tag{62a}$$

$$n(t+\Delta t) = n(t) + (1/2)\,(H(n') + H(n(t)))\Delta t \tag{62b}$$

Modified Euler:

$$n' = n(t) + H(n(t))\Delta t \tag{63a}$$

$$n(t+\Delta t) = n(t) + (1/2)\,(H(n') + H(n(t)))\Delta t \tag{63b}$$

Note that each of these schemes consist of a predictor (62a, 63a) followed by a corrector (62b, 63b), and that the corrector stages are identical. Both schemes are of second order accuracy, meaning that if $n(t)$, $n(t-\Delta t)$, $H(n(t))$, and $H(n(t-\Delta t))$ are known exactly then the error $E(t+\Delta t)$ in the solution $n(t+\Delta t)$ decays as some constant times $\Delta t^2$ as $\Delta t \to 0$:

$$E(t+\Delta t) \to C\,\Delta t^2,\ \Delta t \to 0;\ C = \text{constant} \tag{64}$$

Restating this in the so-called O - notation:

$$E(t+\Delta t) = O(\Delta t^2) \tag{65}$$

The advantage that the modified Euler scheme enjoys is that only $n(t)$ need be known to advance the solution to time $t+\Delta t$, while the leapfrog-trapezoidal scheme requires in addition a knowledge of $n(t-\Delta t)$. However this advantage is outweighed by the fact that the modified Euler scheme is actually weakly unstable for the case $n(t) = e^{i\theta}$, $\theta$ a real number, $H(n) = ikn$, $k$ a positive real number. That is, $|n(t+\Delta t)| > 1$ whereas analytically $|n(t+\Delta t)| = 1$ for all $\Delta t$. This form of $H(n)$ is of great interest since if we set $n(x,t) = e^{i(kx-\omega t)}$ then the convective derivative for unit velocity is $\partial n/\partial x = ikn$. For the continuity equation this instability has the effect of amplifying the short spatial wavelength components of the density field slightly. The leapfrog-trapezoidal scheme does not have this defect, and is therefore the one we have chosen for use in our simulation codes. The modified Euler scheme is used in our codes only to start the calculation from the initial conditions, or to change the time step, which must be done occasionally, since even the leapfrog-trapezoidal scheme is stable only when $\Delta t < \Delta t^{min}$, where $\Delta t^{min}$ depends on the effective value of $k$ produced by the spatial operator $H$.

Our problem has now been reduced to that of evaluating the spatial operator $H$ on the finite difference grid shown in Fig. 7. First we note that

$$H(n) = \nabla_\perp \cdot (n\, \underset{\sim}{v}_{e\perp}) = \partial f/\partial x + \partial g/\partial y \tag{66}$$

where

$$f(n) = n\, v_x(n) \tag{67}$$

$$g(n) = n\, v_y(n) \tag{68}$$

$$\underset{\sim}{v}_{e\perp} = v_x \hat{x} + v_y \hat{y} \tag{69}$$

and $\underset{\sim}{v}_{e\perp}$ is given by Eq. (46). As we stated earlier, $n$ and $\phi$ are given on the mesh points $(x_i, y_j)$ and are denoted by $n_{ij}$ and $\phi_{ij}$ respectively. We shall also evaluate $v_x$ and $v_y$ on these same grid points, using centered finite difference formulae to be given presently. Therefore the quantities $f$ and $g$ above are also known on these grid points. We shall assume for the moment that our mesh is uniform, i.e., that $\Delta x_{i+1/2} \equiv x_{i+1} - x_i$ is independent of $i$ and that $\Delta y_{j+1/2} \equiv y_{j+1} - y_j$ is independent of $j$, and denote these grid spacings by simply $\Delta x$ and $\Delta y$ respectively. Modifications necessary for a nonuniform mesh will be given later. Then we can approximate the quantity $\partial f/\partial x$ to various orders of accuracty:

$$\left(\frac{\partial f}{\partial x}\right)_{ij} = (f_{i+1,j} - f_{ij})/\Delta x + O(\Delta x) \tag{70}$$

$$\left(\frac{\partial f}{\partial x}\right)_{ij} = (f_{i+1,j} - f_{i-1,j})/(2\Delta x) + O(\Delta x^2) \tag{71}$$

$$\left(\frac{\partial f}{\partial x}\right)_{ij} = 2(f_{i+1,j} - f_{i-1,j})/(3\Delta x) - (f_{i+2,j} - f_{i-2,j})/(12\Delta x) + O(\Delta x^4) \tag{72}$$

Similar expressions exist for approximating $\partial g/\partial y$. For instance

$$\left(\frac{\partial g}{\partial y}\right)_{ij} = (g_{i,j+1} - g_{i,j-1})/(2\Delta y) + O(\Delta y^2) \tag{73}$$

Recall that earlier we had assumed that $v_x$ and $v_y$ were known on grid points $(x_i,\ y_j)$. Looking at Eq. (46) and (47) we see that this requires a knowledge of $\nabla_\perp \phi = \partial\phi/\partial x\ \hat{x} + \partial\phi/\partial y\ \hat{y}$ on grid points, which are obtained using the above formulae by substituing $\phi$ for both f and g.

If we simply choose an order of accuracy desired or required for our problem, we have apparently completely specified our solution algorithm; and indeed, for many kinds of problems this would be completely sufficient. However, if one attempts to solve even the simplest of continuity equations ($\partial n/\partial y = 0$, $v_y = 0$, $v_x =$ constant) in the presence of very steep gradients of n in the x direction, the numerical solution is soon seen to be contaminated by the appearance of spurious nonphysical oscillations or "ripples" which can grow in time and eventually destroy all of the information content of the calculation. The reasons are many and varied, but in the final analysis are directly caused by the error associated with the finiteness of $\Delta x$, $\Delta y$, and $\Delta t$: the "discretization error". Often this error can be reduced to acceptable levels simply by using formally more accurate finite difference approximations for spatial and temporal derivatives, for instance by using Eq. (72) instead of Eq. (71), or using a fourth-order Runge Kutta solver to integrate in time instead of our leapfrog-trapezoidal scheme. However, if the spatial or temporal gradients are such that the Taylor series expansion implicit in all finite difference formulae is either nonconvergent or slowly convergent, then this technique will not improve matters appreciably, and may even increase the error. The brute force approach, of course, is to keep reducing $\Delta x$, $\Delta y$ and $\Delta t$ until we resolve all spatial and temporal structure sufficiently well to get a convergent solution. However there are many physical systems, among them the barium cloud and equatorial spread F system, which allow "shock-like" solutions, i.e., solutions which contain regions where the gradient scale length is orders of magnitude smaller that that of the other features in the problem. On the scale of the overall structure of the solution, these regions are well approximated by discontinuities. These discontinuities effect the rest of solution in time solely through their propagation speed ("shock speed") and the change in the physical characteristics and velocity of the plasma across the discontinuity ("jump conditions"). It is obviously impossible in a situation like this to reduce $\Delta x$, $\Delta y$ and $\Delta t$ to the point where the actual structure inside the shock is resolved on our finite difference mesh. Fortunately, it is also unnecessary. In their classic paper, Lax and Wendroff (1960) showed that when these shock-like solutions appeared within the context of a system of conservation laws (mass, momentum, and energy, for example), then any finite difference scheme which could represent the shock as a stable propagating entity, regardless of the computed internal shock structure, would recover the correct shock speed and jump conditions (and thus the correct influence of the shock on the rest of the solution) if it were in conservation form, a term we shall define momentarily. Thus it is sufficient to utilize a scheme which is both in conservation form and which has the property of representing a shock as a stable propagating entity. Within this class of schemes one is usually confronted with a choice between schemes which allow numerical oscillations near the shock front, which may be severe and which may in fact destroy the accuracy of the entire calculation if not carefully controlled, and schemes which artifically smear the shock front over large numbers of grid points. The oscillatory schemes in general are of second or higher order accuracy in time or space, while the dissipative, non-oscillatory schemes are all first order accurate in time and space. We shall therefore use the terms "high order" and "low order" to describe the above oscillatory and non-oscillatory schemes respectively. The choice between high and low order schemes is a particularly unpleasant one. The inherently high numerical dissipation of the low order schemes tends to excessively smooth the other physical structures in the problem as well as the shock front, and the low convergence rate ($O(\Delta x, \Delta y, \Delta t)$) may mean that almost as many grid points may be required for sufficient accuracy as would have been required to actually resolve the shock structure to begin with. On the other hand the numerical oscillations associated with the high order schemes often propagate into the entire domain of the solution, destroying all of the accuracy of the calculation. Again we are fortunate in that we do not have to make this choice, since we can have the best of both schemes by utilizing a technique known as flux-corrected transport (FCT), which was originally developed by Boris and Book (1973) and later generalized by Zalesak (1979).

Consider our continuity equation

$$\partial n/\partial t + \partial f(n)/\partial x + \partial g(n)/\partial y = 0 \qquad (74)$$

We shall say that a finite difference approximation to Eq. (74) is in conservation (or "flux") form when it can be written in the form

$$n_{ij}(t+\Delta t) = n_{ij}(t) - \Delta V_{ij}^{-1} [F_{i+(1/2),j} - F_{i-(1/2),j} + G_{i,j+(1/2)} - G_{i,j-1/2)}] \qquad (75)$$

where $\Delta V_{ij} = \Delta x_i \Delta y_j$ is an area element centered on grid point $(x_i, y_j)$. The $F_{i+(1/2),j}$ and $G_{i,j+(1/2)}$ are called transportive fluxes and are functions of f and g respectively at one or more of the time levels. The functional dependence of F on f and of G on g defines the numerical scheme. For instance, if we choose the trapezoidal corrector step Eq. (62b) combined with fourth order accurate spatial derivatives Eq. (72) then

$$F_{i+(1/2),j} = [\frac{7}{12} (f''_{i+1,j} + f''_{ij}) - \frac{1}{12} (f''_{i+2,j} + f''_{i-1,j})]\Delta y_j \qquad (76)$$

$$f''_{ij} = \frac{1}{2} (f(n'_{ij}) + f(n_{ij}(t))) \qquad (77)$$

The essence of the FCT method is as follows. For each time step one computes two distinct sets of F and G: one set by a low order scheme (the "low order fluxes") and the other set by a high order scheme (the "high order fluxes"). Then at each cell interface (i + (1/2),j) and (i, j+(1/2)) one uses a weighted average of the high and low order flux as the final flux. This weighting is done in a manner which insures that the high order flux is utilized to the greatest extent possible without introducing numerical oscillations in the solution. The solution which would have resulted if the low order scheme had been used alone is used as the standard by which to determine whether an oscillation is numerical or physical. The result is a family of schemes capable of resolving discontinuities over 2 - 3 grid points with very little smearing of other physical details and no numerical oscillations. For more details, see Boris and Book (1973) or Zalesak (1979).

Before closing this section, let us briefly describe our treatment of nonuniform spatial grids. The basic technique is to utilize a smooth mapping from our "grid space" (i,j) to real space (x,y). The mappings we use are especially simple in that x = x(i) and y = y(j). Since our nonuniform spatial mesh enters only in our evaluation of $\partial f/\partial x$ and $g/\partial y$ and since the treatment for each is the same we shall simply show our evaluation of $\partial f/\partial x$ here. Utilizing the dummy index k and treating it as a continuous variable, we simply use the chain rule:

$$\left(\frac{\partial f}{\partial x}\right)_{ij} = \left(\frac{\partial f}{\partial k}\right)_{ij} \left(\frac{\partial k}{\partial x(k)}\right)_i = \left(\frac{\partial f}{\partial k}\right)_{ij} \left(\frac{\partial x}{\partial k}\right)_i^{-1} \tag{78}$$

Now f as a function of the index k is by definition given on a uniform mesh, so we can use all of our previously given formulae for spatial derivatives and fluxes. The derivative $(\partial x/\partial k)_i$ can be taken analytically if we have specified an analytic map from "k-space" to "x-space", or if this map is not given explicity but is still smooth we can again use the previously given formulae for spatial derivatives since x as a function of k is also by definition given on a uniform mesh. In terms of our flux formulation, this simply means that $\Delta x_i$ is defined to be $(\partial x/\partial k)_i$, and the rest of the scheme remains intact.

## 9. Concluding Remarks

We hope to have given the reader an understanding of the basic physics of the plasma instabilities underlying the ionospheric irregularities treated here, as well as of some of the fundamental concepts involved in the numerical integration of the differential equations describing this physics. We cannot treat the subject in its entirety here, but have rather tried to give the reader enough information to get started on his own if he so desires. Both aspects of the subject, the physics and the numerical analysis, are extremely dynamic fields. Of particular interest to this author is the fact that the subject of numerical solutions to continuity equations has recently become an area of widespread intensive study by many researchers. The reader is strongly advised to monitor the relevant numerical and mathematical literature.

### Acknowledgments

This work was sponsored by the Defense Nuclear Agency and the Office of Naval Research.

R-889

Figure 1. Photograph of the Spruce barium cloud 24 minutes after release. Bright areas are ionized barium. The line of sight near the center of the picture is parallel to the magnetic field at the cloud altitude.

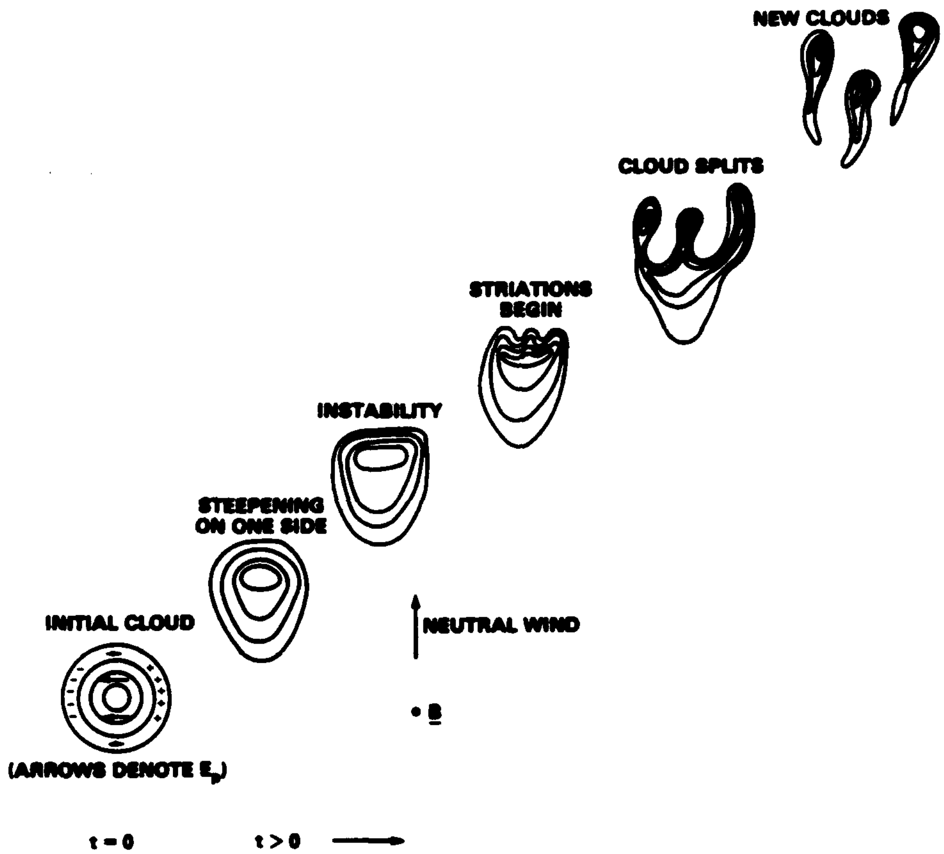


Figure 2. Sketch of the time evolution of a typical barium cloud in a plane perpendicular to the magnetic field, subject to an upward directed neutral wind. Lines demarking the cloud denote plasma density contours, with the highest plasma density in the center of cloud.

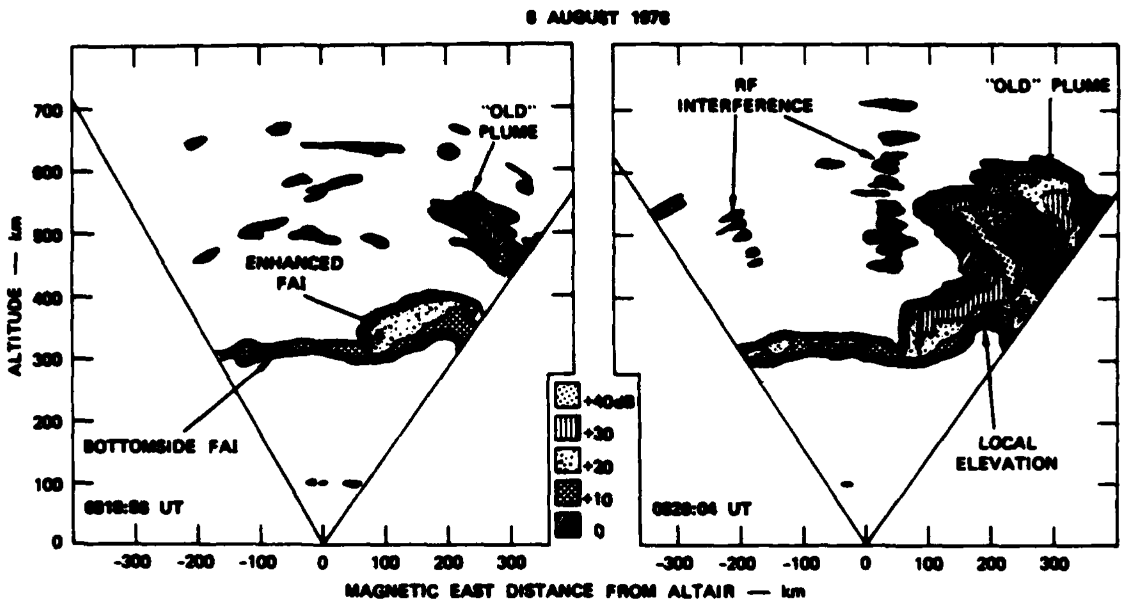


Figure 3. Two sequential maps of 3 meter radar backscatter at the earth's magnetic equator. Regions of intense backscatter have been shown to be associated with regions of severe electron density depletion. From R.T. Tsunoda, J. Geophys. Res., 86, 139, 1981, copyrighted by the American Geophysical Union.

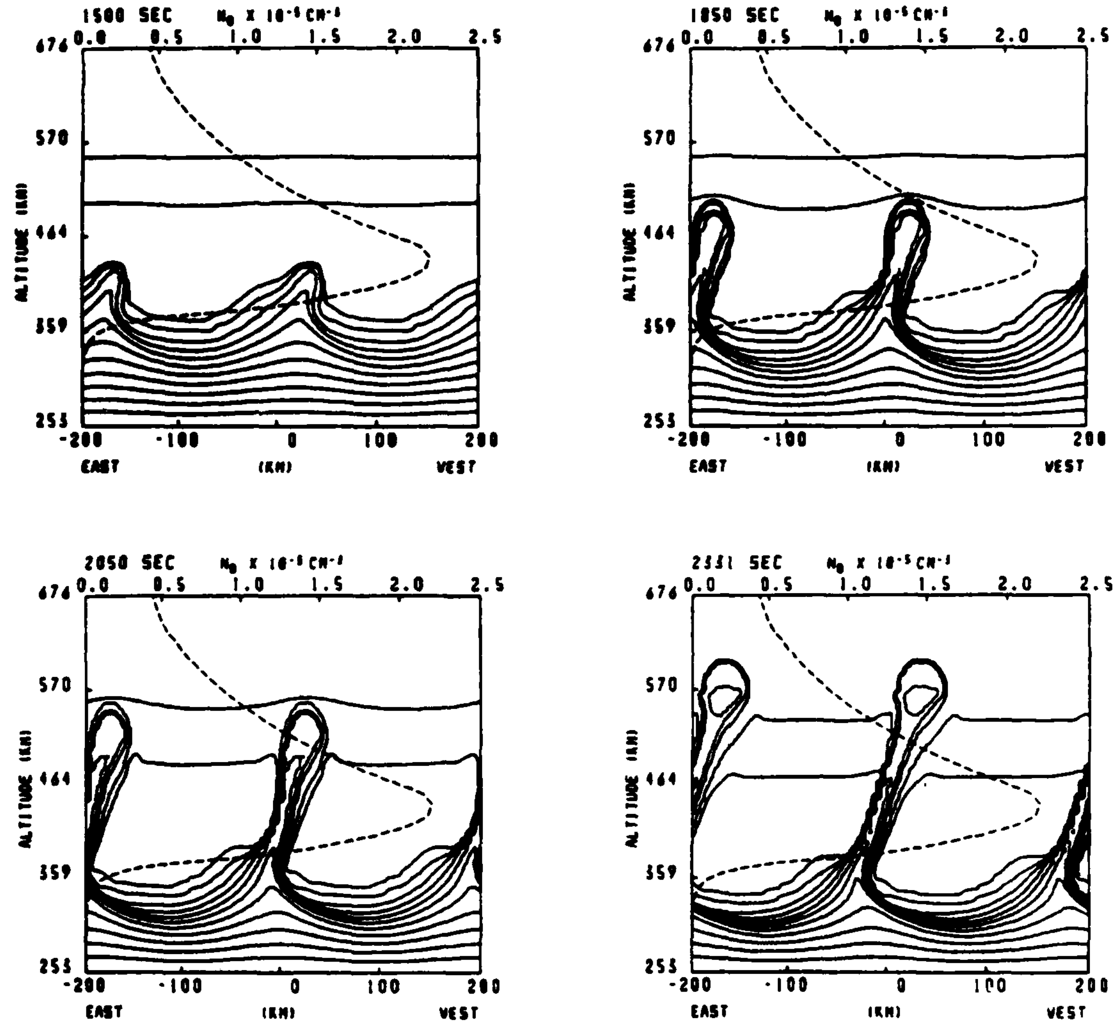


Figure 4. Four sequential plots of contours of electron density at the earth's equator depicting the formation and subsequent buoyant rise of an ESF "bubble", taken from a numerical simulation of Zalesak et al. (1982).

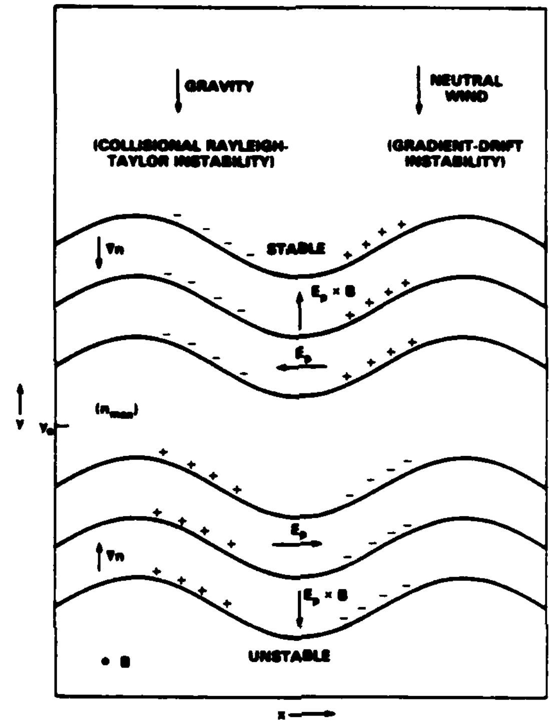


Figure 5. Contours of constant plasma density n for in an x-y plane perpendicular to the magnetic field. n is a function of y which maximizes at $y = y_o$, superimposed on which is a perturbation of the form sin kx, where k is a wavenumber. Either a downward-directed gravity or a downward-directed neutral wind causes ions to shift slightly leftward relative to the electrons, which results in an $\underset{\sim}{E}_p \times \underset{\sim}{B}$ velocity which either damps or enhances the perturbation, depending on the sign of $\partial n/\partial y$.

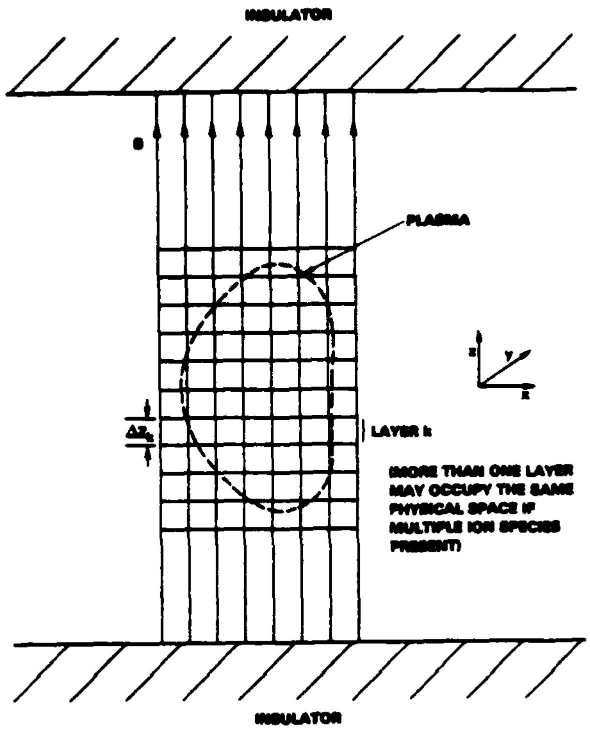


Figure 6. Model of plasma and magnetic field geometry used in this paper. Field lines terminate on insulators at $z = \pm \infty$. Plasma is divided into "layers" along z for mathematical and numerical treatment. Each layer consists of a single ion species and its associated electrons. Multiple collocated ion species are treated by having multiple collocated "layers".

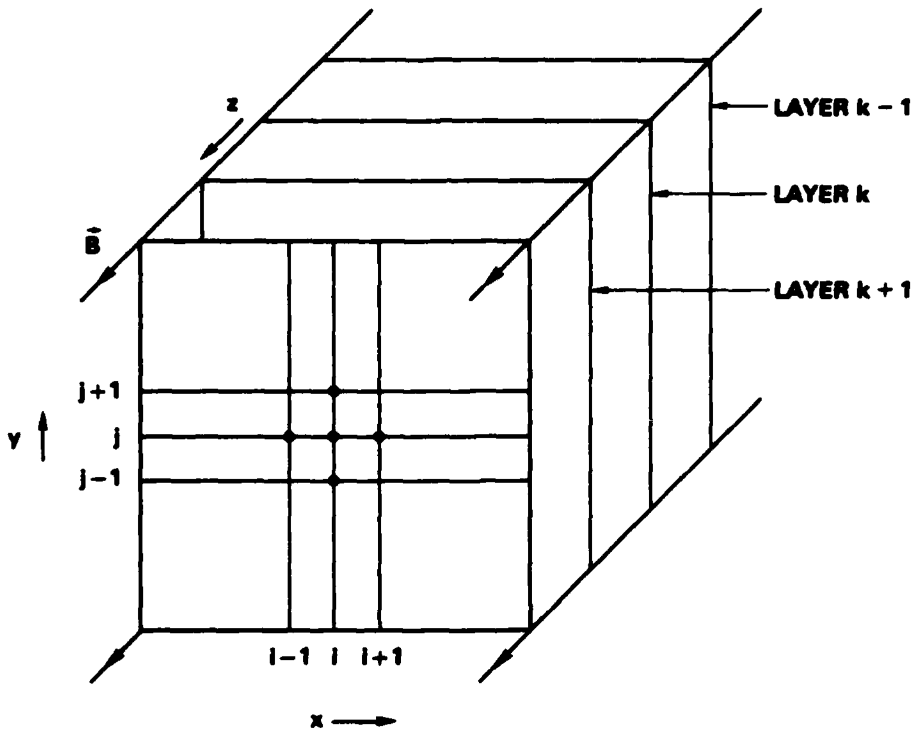


Figure 7. Spatial finite difference grid used in the numerical simulation codes, showing the correspondence between i and x and between j and y. Several layers of plasma are shown, even through the discussion in the text assumes only one layer. Grid points are shown as dots.

## References


Boris, J.P., and Book, D.L.: 1973, J. Comput. Phys., 11, 38.

Hain, K.: 1980, Nav. Res. Lab. Memo. Rep. 4264, Naval Research Laboratory, Washington, D.C.

Kershaw, D.S.: 1979, J. Comput. Phys., 26, 263.

Lax, P., and Wendroff, B.: 1960, Comm. Pure Appl. Math., 13, 217.

Madala, R.V.: 1978, Mon. Weather Rev., 106, 1735.

McDonald, B.E.: 1980, J. Comput. Phys., 35, 147.

Tsunoda, R.T.: 1981, J. Geophys. Res., 86, 139.

Zalesak, S.T.,: 1979, J. Comput. Phys., 31, 335.

Zalesak, S.T., Ossakow, S.L., and Chaturvedi, P.K.: 1982, J. Geophys. Res., 87, 151.

## DISTRIBUTION LIST

**DEPARTMENT OF DEFENSE**

ASSISTANT SECRETARY OF DEFENSE
COMM, CMD, CONT 7 INTELL
WASHINGTON, D.C. 20301

DIRECTOR
COMMAND CONTROL TECHNICAL CENTER
PENTAGON RM BE 685
WASHINGTON, D.C. 20301
01CY ATTN C-650
01CY ATTN C-312 R. MASON

DIRECTOR
DEFENSE ADVANCED RSCH PROJ AGENCY
ARCHITECT BUILDING
1400 WILSON BLVD.
ARLINGTON, VA. 22209
01CY ATTN NUCLEAR MONITORING RESEARCH
01CY ATTN STRATEGIC TECH OFFICE

DEFENSE COMMUNICATION ENGINEER CENTER
1860 WIEHLE AVENUE
RESTON, VA. 22090
01CY ATTN CODE R410
01CY ATTN CODE R812

DEFENSE TECHNICAL INFORMATION CENTER
CAMERON STATION
ALEXANDRIA, VA. 22314
02CY

DIRECTOR
DEFENSE NUCLEAR AGENCY
WASHINGTON, D.C. 20305
01CY ATTN STVL
04CY ATTN TITL
01CY ATTN DDST
03CY ATTN RAAE

COMMANDER
FIELD COMMAND
DEFENSE NUCLEAR AGENCY
KIRTLAND, AFB, NM 87115
01CY ATTN FCPR

DIRECTOR
INTERSERVICE NUCLEAR WEAPONS SCHOOL
KIRTLAND AFB, NM 87115
01CY ATTN DOCUMENT CONTROL

JOINT CHIEFS OF STAFF
WASHINGTON, D.C. 20301
01CY ATTN J-3 WWMCCS EVALUATION OFFICE

DIRECTOR
JOINT STRAT TGT PLANNING STAFF
OFFUTT AFB
OMAHA, NB 68113
01CY ATTN JLTW-2
01CY ATTN JPST G. GOETZ

CHIEF
LIVERMORE DIVISION FLD COMMAND DNA
*DEPARTMENT OF DEFENSE*
LAWRENCE LIVERMORE LABORATORY
P.O. BOX 808
LIVERMORE, CA 94550
01CY ATTN FCPRL

*COMMANDANT*
NATO SCHOOL (SHAPE)
APO NEW YORK 09172
01CY ATTN U.S. DOCUMENTS OFFICER

UNDER SECY OF DEF FOR RSCH & ENGRG
*DEPARTMENT OF DEFENSE*
WASHINGTON, D.C. 20301
01CY ATTN STRATEGIC & SPACE SYSTEMS (OS)

WWMCCS SYSTEM ENGINEERING ORG
WASHINGTON, D.C. 20305
01CY ATTN R. CRAWFORD

COMMANDER/DIRECTOR
ATMOSPHERIC SCIENCES LABORATORY
U.S. ARMY ELECTRONICS COMMAND
WHITE SANDS MISSILE RANGE, NM 88002
01CY ATTN DELAS-EO F. NILES

DIRECTOR
BMD ADVANCED TECH CTR
HUNTSVILLE OFFICE
P.O. BOX 1500
HUNTSVILLE, AL 35807
01CY ATTN ATC-T MELVIN T. CAPPS
01CY ATTN ATC-O W. DAVIES
01CY ATTN ATC-R DON RUSS

PROGRAM MANAGER
BMD PROGRAM OFFICE
5001 EISENHOWER AVENUE
ALEXANDRIA, VA 22333
01CY ATTN DACS-BMT J. SHEA

CHIEF C-E- SERVICES DIVISION
U.S. ARMY COMMUNICATIONS CMD
PENTAGON RM 1B269
WASHINGTON, D.C. 20310
01CY ATTN C- E-SERVICES DIVISION

COMMANDER
FRADCOM TECHNICAL SUPPORT ACTIVITY
DEPARTMENT OF THE ARMY
FORT MONMOUTH, N.J. 07703
01CY ATTN DRSEL-NL-RD H. BENNET
01CY ATTN DRSEL-PL-ENV H. BOMKE
01CY ATTN J.E. QUIGLEY

COMMANDER
U.S. ARMY COMM-ELEC ENGRG INSTAL AGY
FT. HUACHUCA, AZ 85613
01CY ATTN CCC-EMEO GEORGE LANE

COMMANDER
U.S. ARMY FOREIGN SCIENCE & TECH CTR
220 7TH STREET, NE
CHARLOTTESVILLE, VA 22901
01CY ATTN DRXST-SD

COMMANDER
U.S. ARMY MATERIAL DEV & READINESS CMD
5001 EISENHOWER AVENUE
ALEXANDRIA, VA 22333
01CY ATTN DRCLDC J.A. BENDER

COMMANDER
U.S. ARMY NUCLEAR AND CHEMICAL AGENCY
7500 BACKLICK ROAD
BLDG 2073
SPRINGFIELD, VA 22150
01CY ATTN LIBRARY

DIRECTOR
U.S. ARMY BALLISTIC RESEARCH LABORATORY
ABERDEEN PROVING GROUND, MD 21005
01CY ATTN TECH LIBRARY EDWARD BAICY

COMMANDER
U.S. ARMY SATCOM AGENCY
FT. MONMOUTH, NJ 07703
01CY ATTN DOCUMENT CONTROL

COMMANDER
U.S. ARMY MISSILE INTELLIGENCE AGENCY
REDSTONE ARSENAL, AL 35809
01CY ATTN JIM GAMBLE

DIRECTOR
U.S. ARMY TRADOC SYSTEMS ANALYSIS ACTIVITY
WHITE SANDS MISSILE RANGE, NM 88002
01CY ATTN ATAA-SA
01CY ATTN TCC/F. PAYAN JR.
01CY ATTN ATTA-TAC LTC J. HESSE

COMMANDER
NAVAL ELECTRONIC SYSTEMS COMMAND
WASHINGTON, D.C. 20360
01CY ATTN NAVALEX 034 T. HUGHES
01CY ATTN PME 117
01CY ATTN PME 117-T
01CY ATTN CODE 5011

COMMANDING OFFICER
NAVAL INTELLIGENCE SUPPORT CTR
4301 SUITLAND ROAD, BLDG. 5
WASHINGTON, D.C. 20390
01CY ATTN MR. DUBBIN STIC 12
01CY ATTN NISC-50
01CY ATTN CODE 5404 J. GALET

COMMANDER
NAVAL OCCEAN SYSTEMS CENTER
SAN DIEGO, CA 92152
01CY ATTN J. FERGUSON

NAVAL RESEARCH LABORATORY
WASHINGTON, D.C. 20375
01CY ATTN CODE 4700 S. L. Ossakow
26 CYS IF UNCLASS. 1 CY IF CLASS)
01CY ATTN CODE 4701 I Vitkovitsky
01CY ATTN CODE 4780 BRANCH HEAD (100
CYS IF UNCLASS, 1 CY IF CLASS)
01CY ATTN CODE 7500
01CY ATTN CODE 7550
01CY ATTN CODE 7580
01CY ATTN CODE 7551
01CY ATTN CODE 7555
01CY ATTN CODE 4730 E. MCLEAN
01CY ATTN CODE 4108
01CY ATTN CODE 4730 B. RIPIN
22CY ATTN CODE 2628

COMMANDER
NAVAL SEA SYSTEMS COMMAND
WASHINGTON, D.C. 20362
01CY ATTN CAPT R. PITKIN

COMMANDER
NAVAL SPACE SURVEILLANCE SYSTEM
DAHLGREN, VA 22448
01CY ATTN CAPT J.H. BURTON

OFFICER-IN-CHARGE
NAVAL SURFACE WEAPONS CENTER
WHITE OAK, SILVER SPRING, MD 20910
01CY ATTN CODE F31

DIRECTOR
STRATEGIC SYSTEMS PROJECT OFFICE
DEPARTMENT OF THE NAVY
WASHINGTON, D.C. 20376
01CY ATTN NSP-2141
01CY ATTN NSSP-2722 FRED WIMBERLY

COMMANDER
NAVAL SURFACE WEAPONS CENTER
DAHLGREN LABORATORY
DAHLGREN, VA 22448
01CY ATTN CODE DF-14 R. BUTLER

OFFICER OF NAVAL RESEARCH
ARLINGTON, VA 22217
01CY ATTN CODE 465
01CY ATTN CODE 461
01CY ATTN CODE 402
01CY ATTN CODE 420
01CY ATTN CODE 421

COMMANDER
AEROSPACE DEFENSE COMMAND/DC
DEPARTMENT OF THE AIR FORCE
ENT AFB, CO 80912
01CY ATTN DC MR. LONG

COMMANDER
AEROSPACE DEFENSE COMMAND/XPD
DEPARTMENT OF THE AIR FORCE
ENT AFB, CO 80912
01CY ATTN XPDQQ
01CY ATTN XP

AIR FORCE GEOPHYSICS LABORATORY
HANSCOM AFB, MA 01731
01CY ATTN OPR HAROLD GARDNER
01CY ATTN LKB KENNETH S.W. CHAMPION
01CY ATTN OPR ALVA T. STAIR
01CY ATTN PHD JURGEN BUCHAU
01CY ATTN PHD JOHN P. MULLEN

AF WEAPONS LABORATORY
KIRTLAND AFT, NM 87117
01CY ATTN SUL
01CY ATTN CA ARTHUR H. GUENTHER
01CY ATTN NTYCE 1LT. G. KRAJEI

AFTAC
PATRICK AFB, FL 32925
01CY ATTN TF/MAJ WILEY
01CY ATTN TN

AIR FORCE AVIONICS LABORATORY
WRIGHT-PATTERSON AFB, OH 45433
01CY ATTN AAD WADE HUNT
01CY ATTN AAD ALLEN JOHNSON

DEPUTY CHIEF OF STAFF
RESEARCH, DEVELOPMENT, & ACQ
DEPARTMENT OF THE AIR FORCE
WASHINGTON, D.C. 20330
01CY ATTN AFRDQ

HEADQUATERS
ELECTRONIC SYSTEMS DIVISION/XR
DEPARTMENT OF THE AIR FORCE
HANSCOM AFB, MA 01731
01CY ATTN XR J. DEAS

HEADQUATERS
ELECTRONIC SYSTEMS DIVISION/YSEA
DEPARTMENT OF THE AIR FORCE
HANSCOM AFB, MA 01732
01CY ATTN YSEA

HEADQUARTERS
ELECTRONIC SYSTEMS DIVISION/DC
DEPARTMENT OF THE AIR FORCE
HANSCOM AFB, MA 01731
01CY ATTN DCKC MAJ J.C. CLARK

COMMANDER
FOREIGN TECHNOLOGY DIVISION, AFSC
WRIGHT-PATTERSON AFB, OH 45433
01CY ATTN NICD LIBRARY
01CY ATTN ETDP B. BALLARD

COMMANDER
ROME AIR DEVELOPMENT CENTER, AFSC
GRIFFISS AFB, NY 13441
01CY ATTN DOC LIBRARY/TSLD
01CY ATTN OCSE V. COYNE

SAMSO/SZ
POST OFFICE BOX 92960
WORLDWAY POSTAL CENTER
LOS ANGELES, CA 90009
(SPACE DEFENSE SYSTEMS)
01CY ATTN SZJ

STRATEGIC AIR COMMAND/XPFS
OFFUTT AFB, NB 68113
01CY ATTN ADWATE MAJ BRUCE BAUER
01CY ATTN NRT
01CY ATTN DOK CHIEF SCIENTIST

SAMSO/SK
P.O. BOX 92960
WORLDWAY POSTAL CENTER
LOS ANGELES, CA 90009
01CY ATTN SKA (SPACE COMM SYSTEMS)
M. CLAVIN

SAMSO/MN
NORTON AFB, CA 92409
(MINUTEMAN)
01CY ATTN MNNL

COMMANDER
ROME AIR DEVELOPMENT CENTER, AFSC
HANSCOM AFB, MA 01731
01CY ATTN EEP A. LORENTZEN

DEPARTMENT OF ENERGY
LIBRARY ROOM G-042
WASHINGTON, D.C. 20545
01CY ATTN DOC CON FOR A. LABOWITZ

DEPARTMENT OF ENERGY
ALBUQUERQUE OPERATIONS OFFICE
P.O. BOX 5400
ALBUQUERQUE, NM 87115
01CY ATTN DOC CON FOR D. SHERWOOD

EG&G, INC.
LOS ALAMOS DIVISION
P.O. BOX 809
LOS ALAMOS, NM 85544
01CY ATTN DOC CON FOR J. BREEDLOVE

UNIVERSITY OF CALIFORNIA
LAWRENCE LIVERMORE LABORATORY
P.O. BOX 808
LIVERMORE, CA 94550
01CY ATTN DOC CON FOR TECH INFO DEPT
01CY ATTN DOC CON FOR L-389 R. OTT
01CY ATTN DOC CON FOR L-31 R. HAGER
01CY ATTN DOC CON FOR L-46 F. SEWARD

LOS ALAMOS NATIONAL LABORATORY
P.O. BOX 1663
LOS ALAMOS, NM 87545
01CY ATTN DOC CON FOR J. WOLCOTT
01CY ATTN DOC CON FOR R.F. TASCHEK
01CY ATTN DOC CON FOR E. JONES
01CY ATTN DOC CON FOR J. MALIK
01CY ATTN DOC CON FOR R. JEFFRIES
01CY ATTN DOC CON FOR J. ZINN
01CY ATTN DOC CON FOR P. KEATON
01CY ATTN DOC CON FOR D. WESTERVELT

SANDIA LABORATORIES
P.O. BOX 5800
ALBUQUERQUE, NM 87115
01CY ATTN DOC CON FOR W. BROWN
01CY ATTN DOC CON FOR A. THORNBROUGH
01CY ATTN DOC CON FOR T. WRIGHT
01CY ATTN DOC CON FOR D. DAHLGREN
01CY ATTN DOC CON FOR 3141
01CY ATTN DOC CON FOR SPACE PROJECT DIV

SANDIA LABORATORIES
LIVERMORE LABORATORY
P.O. BOX 969
LIVERMORE, CA 94550
01CY ATTN DOC CON FOR B. MURPHEY
01CY ATTN DOC CON FOR T. COOK

OFFICE OF MILITARY APPLICATION
DEPARTMENT OF ENERGY
WASHINGTON, D.C. 20545
01CY ATTN DOC CON DR. YO SONG

OTHER GOVERNMENT

DEPARTMENT OF COMMERCE
NATIONAL BUREAU OF STANDARDS
WASHINGTON, D.C. 20234
(ALL CORRES: ATTN SEC OFFICER FOR)
01CY ATTN R. MOORE

INSTITUTE FOR TELECOM SCIENCES
NATIONAL TELECOMMUNICATIONS & INFO ADMIN
BOULDER, CO 80303
01CY ATTN A. JEAN (UNCLASS ONLY)
01CY ATTN W. UTLAUT
01CY ATTN D. CROMBIE
01CY ATTN L. BERRY

NATIONAL OCEANIC & ATMOSPHERIC ADMIN
ENVIRONMENTAL RESEARCH LABORATORIES
DEPARTMENT OF COMMERCE
BOULDER, CO 80302
01CY ATTN R. GRUBB
01CY ATTN AERONOMY LAB G. REID

DEPARTMENT OF DEFENSE CONTRACTORS

AEROSPACE CORPORATION
P.O. BOX 92957
LOS ANGELES, CA 90009
01CY ATTN I. GARFUNKEL
01CY ATTN T. SALMI
01CY ATTN V. JOSEPHSON
01CY ATTN S. BOWER
01CY ATTN D. OLSEN

ANALYTICAL SYSTEMS ENGINEERING CORP
5 OLD CONCORD ROAD
BURLINGTON, MA 01803
01CY ATTN RADIO SCIENCES

AUSTIN RESEARCH ASSOC., INC.
1901 RUTLAND DRIVE
AUSTIN, TX 78758
01CY ATTN L. SLOAN
01CY ATTN R. THOMPSON

BERKELEY RESEARCH ASSOCIATES, INC.
P.O. BOX 983
BERKELEY, CA 94701
01CY ATTN J. WORKMAN
01CY ATTN C. PRETTIE
01CY ATTN S. BRECHT

BOEING COMPANY, THE
P.O. BOX 3707
SEATTLE, WA 98124
01CY ATTN G. KEISTER
01CY ATTN D. MURRAY
01CY ATTN G. HALL
01CY ATTN J. KENNEY

CALIFORNIA AT SAN DIEGO, UNIV OF
P.O. BOX 6049
SAN DIEGO, CA 92106
CHARLES STARK DRAPER LABORATORY, INC.
555 TECHNOLOGY SQUARE
CAMBRIDGE, MA 02139
01CY ATTN D.B. COX
01CY ATTN J.P. GILMORE

COMSAT LABORATORIES
LINTHICUM ROAD
CLARKSBURG, MD 20734
01CY ATTN G. HYDE

CORNELL UNIVERSITY
DEPARTMENT OF ELECTRICAL ENGINEERING
ITHACA, NY 14850
01CY ATTN D.T. FARLEY, JR.

ELECTROSPACE SYSTEMS, INC.
BOX 1359
RICHARDSON, TX 75080
01CY ATTN H. LOGSTON
01CY ATTN SECURITY (PAUL PHILLIPS)

EOS TECHNOLOGIES, INC.
606 Wilshire Blvd.
Santa Monica, Calif 90401
01CY ATTN C.B. GABBARD

ESL, INC.
495 JAVA DRIVE
SUNNYVALE, CA 94086
01CY ATTN J. ROBERTS
01CY ATTN JAMES MARSHALL

GENERAL ELECTRIC COMPANY
SPACE DIVISION
VALLEY FORGE SPACE CENTER
GODDARD BLVD KING OF PRUSSIA
P.O. BOX 8555
PHILADELPHIA, PA 19101
01CY ATTN M.H. BORTNER SPACE SCI LAB

GENERAL ELECTRIC COMPANY
P.O. BOX 1122
SYRACUSE, NY 13201
01CY ATTN F. REIBERT

GENERAL ELECTRIC TECH SERVICES CO., INC.
HMES
COURT STREET
SYRACUSE, NY 13201
  01CY ATTN G. MILLMAN

GEOPHYSICAL INSTITUTE
UNIVERSITY OF ALASKA
FAIRBANKS, AK 99701
  (ALL CLASS ATTN: SECURITY OFFICER)
  01CY ATTN T.N. DAVIS (UNCLASS ONLY)
  01CY ATTN TECHNICAL LIBRARY
  01CY ATTN NEAL BROWN (UNCLASS ONLY)

GTE SYLVANIA, INC.
ELECTRONICS SYSTEMS GRP-EASTERN DIV
77 A STREET
NEEDHAM, MA 02194
  01CY ATTN DICK STEINHOF

HSS, INC.
2 ALFRED CIRCLE
BEDFORD, MA 01730
  01CY ATTN DONALD HANSEN

ILLINOIS, UNIVERSITY OF
107 COBLE HALL
150 DAVENPORT HOUSE
CHAMPAIGN, IL 61820
  (ALL CORRES ATTN DAN MCCLELLAND)
  01CY ATTN K. YEH

INSTITUTE FOR DEFENSE ANALYSES
1801 NO. BEAUREGARD STREET
ALEXANDRIA, VA 22311
  01CY ATTN J.M. AEIN
  01CY ATTN ERNEST BAUER
  01CY ATTN HANS WOLFARD
  01CY ATTN JOEL BENGSTON

INTL TEL & TELEGRAPH CORPORATION
500 WASHINGTON AVENUE
NUTLEY, NJ 07110
  01CY ATTN TECHNICAL LIBRARY

JAYCOR
11011 TORREYANA ROAD
P.O. BOX 85154
SAN DIEGO, CA 92138
  01CY ATTN J.L. SPERLING

JOHNS HOPKINS UNIVERSITY
APPLIED PHYSICS LABORATORY
JOHNS HOPKINS ROAD
LAUREL, MD 20810
  01CY ATTN DOCUMENT LIBRARIAN
  01CY ATTN THOMAS POTEMRA
  01CY ATTN JOHN DASSOULAS

KAMAN SCIENCES CORP
P.O. BOX 7463
COLORADO SPRINGS, CO 80933
  01CY ATTN T. MEAGHER

KAMAN TEMPO-CENTER FOR ADVANCED STUDIES
816 STATE STREET (P.O DRAWER QQ)
SANTA BARBARA, CA 93102
  01CY ATTN DASIAC
  01CY ATTN WARREN S. KNAPP
  01CY ATTN WILLIAM MCNAMARA
  01CY ATTN B. GAMBILL

LINKABIT CORP
10453 ROSELLE
SAN DIEGO, CA 92121
  01CY ATTN IRWIN JACOBS

LOCKHEED MISSILES & SPACE CO., INC
P.O. BOX 504
SUNNYVALE, CA 94088
  01CY ATTN DEPT 60-12
  01CY ATTN D.R. CHURCHILL

LOCKHEED MISSILES & SPACE CO., INC.
3251 HANOVER STREET
PALO ALTO, CA 94304
  01CY ATTN MARTIN WALT DEPT 52-12
  01CY ATTN W.L. IMHOF DEPT 52-12
  01CY ATTN RICHARD G. JOHNSON DEPT 52-12
  01CY ATTN J.B. CLADIS DEPT 52-12

MARTIN MARIETTA CORP
ORLANDO DIVISION
P.O. BOX 5837
ORLANDO, FL 32805
  01CY ATTN R. HEFFNER

M.I.T. LINCOLN LABORATORY
P.O. BOX 73
LEXINGTON, MA 02173
  01CY ATTN DAVID M. TOWLE
  01CY ATTN L. LOUGHLIN
  01CY ATTN D. CLARK

MCDONNEL DOUGLAS CORPORATION
5301 BOLSA AVENUE
HUNTINGTON BEACH, CA 92647
01CY ATTN N. HARRIS
01CY ATTN J. MOULE
01CY ATTN GEORGE MROZ
01CY ATTN W. OLSON
01CY ATTN R.W. HALPRIN
01CY ATTN TECHNICAL LIBRARY SERVICES

MISSION RESEARCH CORPORATION
735 STATE STREET
SANTA BARBARA, CA 93101
01CY ATTN P. FISCHER
01CY ATTN W.F. CREVIER
01CY ATTN STEVEN L. GUTSCHE
01CY ATTN D. SAPPENFIELD
01CY ATTN R. BOGUSCH
01CY ATTN R. HENDRICK
01CY ATTN RALPH KILB
01CY ATTN DAVE SOWLE
01CY ATTN F. FAJEN
01CY ATTN M. SCHEIBE
01CY ATTN CONRAD L. LONGMIRE
01CY ATTN B. WHITE

MISSION RESEARCH CORP.
1400 SAN MATEO BLVD. SE
SUITE A
ALBUQUERQUE, NEW MEXICO 87108
01CY R. STELLINGWERF
01CY M. ALME
01CY L. WRIGHT

MITRE CORPORATION, THE
P.O. BOX 208
BEDFORD, MA 01730
01CY ATTN JOHN MORGANSTERN
01CY ATTN G. HARDING
01CY ATTN C.E. CALLAHAN

MITRE CORP
WESTGATE RESEARCH PARK
1820 DOLLY MADISON BLVD
MCLEAN, VA 22101
01CY ATTN W. HALL
01CY ATTN W. FOSTER

PACIFIC-SIERRA RESEARCH CORP
12340 SANTA MONICA BLVD.
LOS ANGELES, CA 90025
01CY ATTN E.C. FIELD, JR.

PENNSYLVANIA STATE UNIVERSITY
IONOSPHERE RESEARCH LAB
318 ELECTRICAL ENGINEERING EAST
UNIVERSITY PARK, PA 16802
(NO CLASS TO THIS ADDRESS)
01CY ATTN IONOSPHERIC RESEARCH LAB

PHOTOMETRICS, INC.
4 ARROW DRIVE
WOBURN, MA 01801
01CY ATTN IRVING L. KOFSKY

PHYSICAL DYNAMICS, INC.
P.O. BOX 3027
BELLEVUE, WA 98009
01CY ATTN E.J. FREMOUW

PHYSICAL DYNAMICS, INC.
P.O. BOX 10367
OAKLAND, CA 94610
ATTN A. THOMSON

R & D ASSOCIATES
P.O. BOX 9695
MARINA DEL REY, CA 90291
01CY ATTN FORREST GILMORE
01CY ATTN WILLIAM B. WRIGHT, JR.
01CY ATTN ROBERT F. LELEVIER
01CY ATTN WILLIAM J. KARZAS
01CY ATTN H. ORY
01CY ATTN C. MACDONALD
01CY ATTN R. TURCO
01CY ATTN L. DeRAND
01CY ATTN W. TSAI

RAND CORPORATION, THE
1700 MAIN STREET
SANTA MONICA, CA 90406
01CY ATTN CULLEN CRAIN
01CY ATTN ED BEDROZIAN

RAYTHEON CO.
528 BOSTON POST ROAD
SUDBURY, MA 01776
01CY ATTN BARBARA ADAMS

RIVERSIDE RESEARCH INSTITUTE
80 WEST END AVENUE
NEW YORK, NY 10023
01CY ATTN VINCE TRAPANI

SCIENCE APPLICATIONS, INC.
P.O. BOX 2351
LA JOLLA, CA 92038
  01CY ATTN LEWIS M. LINSON
  01CY ATTN DANIEL A. HAMLIN
  01CY ATTN E. FRIEMAN
  01CY ATTN E.A. STRAKER
  01CY ATTN CURTIS A. SMITH
  01CY ATTN JACK MCDOUGALL

SCIENCE APPLICATIONS, INC
1710 GOODRIDGE DR.
MCLEAN, VA 22102
  ATTN: J. COCKAYNE

SRI INTERNATIONAL
333 RAVENSWOOD AVENUE
MENLO PARK, CA 94025
  01CY ATTN DONALD NEILSON
  01CY ATTN ALAN BURNS
  01CY ATTN G. SMITH
  01CY ATTN R. TSUNODA
  01CY ATTN DAVID A. JOHNSON
  01CY ATTN WALTER G. CHESNUT
  01CY ATTN CHARLES L. RINO
  01CY ATTN WALTER JAYE
  01CY ATTN J. VICKREY
  01CY ATTN RAY L. LEADABRAND
  01CY ATTN G. CARPENTER
  01CY ATTN G. PRICE
  01CY ATTN J. PETERSON
  01CY ATTN R. LIVINGSTON
  01CY ATTN V. GONZALES
  01CY ATTN D. MCDANIEL

STEWART RADIANCE LABORATORY
UTAH STATE UNIVERSITY
1 DE ANGELO DRIVE
BEDFORD, MA 01730
  01CY ATTN J. ULWICK

TECHNOLOGY INTERNATIONAL CORP
75 WIGGINS AVENUE
BEDFORD, MA 01730
  01CY ATTN W.P. BOQUIST

TOYON
34 WALNUT LAND
SANTA BARBARA, CA 93111
  01CY ATTN JOHN ISE, JR.
  01CY ATTN JOEL GARBARINO

TRW DEFENSE & SPACE SYS GROUP
ONE SPACE PARK
REDONDO BEACH, CA 9C?78
  01CY ATTN R. K. PLEBUCH
  01CY ATTN S. ALTSCHULER
  01CY ATTN D. DEE
  01CY ATTN D. STOCKWELL
  SNTF/1575

VISIDYNE
SOUTH BEDFORD STREET
BURLINGTON, MASS 01803
  01CY ATTN W. REIDY
  01CY ATTN J. CARPENTER
  01CY ATTN C. HUMPHREY

IONOSPHERIC MODELING DISTRIBUTION LIST
(UNCLASSIFIED ONLY)

PLEASE DISTRIBUTE ONE COPY TO EACH OF THE FOLLOWING PEOPLE (UNLESS OTHERWISE NOTED)

NAVAL RESEARCH LABORATORY
WASHINGTON, D.C. 20375
DR. P. MANGE - CODE 4101
DR. E. SZUSZCZEWICZ - CODE 4108
DR. J. GOODMAN - CODE 4180
DR. P. RODRIGUEZ - CODE 4108

A.F. GEOPHYSICS LABORATORY
L.G. HANSCOM FIELD
BEDFORD, MA 01730
DR. T. ELKINS
DR. W. SWIDER
MRS. R. SAGALYN
DR. J.M. FORBES
DR. T.J. KENESHEA
DR. W. BURKE
DR. H. CARLSON
DR. J. JASPERSE

BOSTON UNIVERSITY
DEPARTMENT OF ASTRONOMY
BOSTON, MA 02215
DR. J. AARONS

CORNELL UNIVERSITY
ITHACA, NY 14850
DR. W.E. SWARTZ
DR. R. SUDAN
DR. D. FARLEY
DR. M. KELLEY

HARVARD UNIVERSITY
HARVARD SQUARE
CAMBRIDGE, MA 02138
DR. M.B. McELROY
DR. R. LINDZEN

INSTITUTE FOR DEFENSE ANALYSIS
400 ARMY/NAVY DRIVE
ARLINGTON, VA 22202
DR. E. BAUER

MASSACHUSETTS INSTITUTE OF TECHNOLOGY
PLASMA FUSION CENTER
LIBRARY, NW16-262
CAMBRIDGE, MA 02139

NASA
GODDARD SPACE FLIGHT CENTER
GREENBELT, MD 20771
DR. R.F. BENSON
DR. K. MAEDA
Dr. S. CURTIS
Dr. M. DUBIN
DR. N. MAYNARD - CODE 696

NATIONAL TECHNICAL INFORMATION CENTER
CAMERON STATION
ALEXANDRIA, VA 22314
12CY ATTN TC

COMMANDER
NAVAL AIR SYSTEMS COMMAND
DEPARTMENT OF THE NAVY
WASHINGTON, D.C. 20360
DR. T. CZUBA

COMMANDER
NAVAL OCEAN SYSTEMS CENTER
SAN DIEGO. CA 92152
MR. R. ROSE - CODE 5321

NOAA
DIRECTOR OF SPACE AND ENVIRONMENTAL LABORATORY
BOULDER, CO 80302
DR. A. GLENN JEAN
DR. G.W. ADAMS
DR. D.N. ANDERSON
DR. K. DAVIES
DR. R. F. DONNELLY

OFFICE OF NAVAL RESEARCH
800 NORTH QUINCY STREET
ARLINGTON, VA 22217
DR. G. JOINER

PENNSYLVANIA STATE UNIVERSITY
UNIVERSITY PARK, PA 16802
DR. J.S. NISBET
DR. P.R. ROHRBAUGH
DR. L.A. CARPENTER
DR. M. LEE
DR. R. DIVANY
DR. P. BENNETT
DR. F. KLEVANS

PRINCETON UNIVERSITY
PLASMA PHYSICS LABORATORY
PRINCETON, NJ 08540
DR. F. PERKINS

SCIENCE APPLICATIONS, INC.
1150 PROSPECT PLAZA
LA JOLLA, CA 92037
DR. D.A. HAMLIN
DR. L. LINSON
DR. E. FRIEMAN

STANFORD UNIVERSITY
STANFORD, CA 94305
DR. P.M. BANKS

U.S. ARMY ABERDEEN RESEARCH
AND DEVELOPMENT CENTER
BALLISTIC RESEARCH LABORATORY
ABERDEEN, MD
DR. J. HEIMERL

GEOPHYSICAL INSTITUTE
UNIVERSITY OF ALASKA
FAIRBANKS, AK 99701
DR. L.C. LEE

UNIVERSITY OF CALIFORNIA,
BERKELEY
BERKELEY, CA 94720
DR. M. HUDSON

UNIVERSITY OF CALIFORNIA
LOS ALAMOS SCIENTIFIC LABORATORY
J-10, MS-664
LOS ALAMOS, NM 87545
DR. M. PONGRATZ
DR. D. SIMONS
DR. G. BARASCH
DR. L. DUNCAN
DR. P. BERNHARDT
DR. S.P. GARY

UNIVERSITY OF CALIFORNIA,
LOS ANGELES
405 HILLGARD AVENUE
LOS ANGELES, CA 90024
DR. F.V. CORONITI
DR. C. KENNEL
DR. A.Y. WONG

UNIVERSITY OF MARYLAND
COLLEGE PARK, MD 20740
DR. K. PAPADOPOULOS
DR. E. OTT

JOHNS HOPKINS UNIVERSITY
APPLIED PHYSICS LABORATORY
JOHNS HOPKINS ROAD
LAUREL, MD 20810
DR. R. GREENWALD
DR. C. MENG

UNIVERSITY OF PITTSBURGH
PITTSBURGH, PA 15213
DR. N. ZABUSKY
DR. M. BIONDI
DR. E. OVERMAN

UNIVERSITY OF TEXAS
AT DALLAS
CENTER FOR SPACE SCIENCES
P.O. BOX 688
RICHARDSON, TEXAS 75080
DR. R. HEELIS
DR. W. HANSON
DR. J.P. McCLURE

UTAH STATE UNIVERSITY
4TH AND 8TH STREETS
LOGAN, UTAH 84322
DR. R. HARRIS
DR. K. BAKER
DR. R. SCHUNK
DR. J. ST.-MAURICE

KIRUNA GEOPHYSICAL INSTITUTE
BOX 709
S-98127 KIRUNA, SWEDEN
CHRISTER JUREN